Environ. Sci. Technol. **2001**, *35,* 3326−3331

Colloid Transport and Deposition in Water-Saturated Yucca Mountain Tuff As Determined by Ionic Strength

AMY P. GAMERDINGER*

Department of Chemistry and Center for Multiphase Environmental Research, Washington State University, Tri-Cities, Richland, Washington 99352, and Applied Geology and Geochemistry, Pacific Northwest National Laboratory, Richland, Washington

DANIEL I. KAPLAN

Savannah River Technology Center, Westinghouse Savannah River Company, Building 773-43a, Room 215, Aiken, South Carolina 29808

Colloid mobility and deposition were determined in model systems consisting of quartz sand or crushed Yucca Mountain tuff, latex microspheres (colloidal particles), and simulated groundwater. Ionic strength (*I*) was manipulated as a first step in defining limiting conditions for colloid transport in a system modeled after geochemical conditions at the Yucca Mountain site. Solutions of deionized water (DI), 0.1×, 1×, and 10× (the ionic strength of simulated groundwater) ($I = 0.0116$ M) were used in saturated columns under steady-state flow conditions. Separate experiments with conservative tracers indicated stable hydrodynamic conditions that were independent of *I*. Colloids were completely mobile (no deposition) in the DI and 0.1× solutions; deposition increased to 11−13% for 1× and to 89−97% for 10× treatments with similar results for sand and tuff. Deposition was described as a pseudo-first-order process; however, a decreasing rate of deposition was apparent for colloid transport at the 10× condition through the tuff. A linear dependence of colloid removal (extent and deposition rate coefficient) on *I* is illustrated for the model Yucca Mountain system and for a glass−KCl system reported in the literature. This simple relationship for saturated systems may be useful for predicting deposition efficiencies under conditions of varying ionic strength.

Introduction

The general importance of colloids and the potential for altering subsurface transport is well-established (*1*). Colloid-facilitated transport of radionuclides has been demonstrated in laboratory experiments (*2*), implicated in field studies (*3*−*7*), and is taken under consideration in designing nuclear waste repositories (*8*). Evaluating the potential threat of colloid-facilitated transport of radionuclides at the site of the proposed nuclear waste repository, Yucca Mountain, NV, is especially difficult due in part to the complexity and uncertainty associated with the geometry of the fractured system and the extremely long period of concern, tens of thousands of years. The tuff surrounding the proposed spent fuel and high-level waste repository contains flow paths through porous matrix interspersed with fractures and faults (*9*).

The chemical composition of the groundwater will affect colloid transport. The plume chemistry is expected to change as it migrates from the near-field, where engineered barriers will control water chemistry, to the far-field, where the solubility of the site's natural minerals will control water chemistry. The plume chemistry of leachates from near-field materials such as glass and cement is expected to vary greatly; *I* may range between 1 and 0.01 M (*10*). The chemistry of the far-field contaminant plume will approach that of the nearby uncontaminated groundwater. The groundwater at the Yucca Mountain site has a typical pH between 7 and 8, an *I* of ∼0.01 M, an oxidizing environment with respect to Fe(II), and is dominated by sodium and bicarbonate ions (*11*).

The increased deposition of particles (*12*) and colloids (*13*−*16*) with increasing *I* is well-established. This trend is consistent with theory; however, deposition during transport for so-called "unfavorable" chemical conditions (where repulsive double-layer interactions dominate the total interaction energy) consistently exceeds that which is predicted by DLVO theory (*14*). Various semiempirical approaches have been taken to improve predictions (*17, 18*).

The primary objective of this research was to identify limiting conditions for colloid transport in crushed tuff material from Yucca Mountain and an aqueous solution matrix based on simulated groundwater. Because of the importance of ionic strength in determining colloid transport and the expected range from the near-field to the far-field, *I* was manipulated in an effort to define conditions for >90% mobility and deposition, respectively. For practical reasons, this research was conducted in a saturated porous matrix, which may be relevant to episodic, saturated flow events (e.g., during periods of increased recharge from storms). The importance of unsaturated flow conditions is recognized and considered in another manuscript. Quartz sand is commonly used as a stationary solid in model systems and was used here as a basis for evaluating the effect of the solid surface on colloid deposition. Electrophoretic mobility of colloids, sand, and tuff was determined to characterize surface charge and to provide a basis for comparison with natural materials and other model systems. Colloid settling experiments were conducted to determine colloid removal from solution by coagulation. The critical coagulation concentration, CCC, was determined to define the ionic strength at which colloids would be removed from solution regardless of transport and deposition.

Experimental Section

Materials. A quartz sand with trace amounts of mica impurities (Accusand, Unimin Corp.) was sieved between 20 and 30 mesh (0.590−0.850 mm), washed with deionized water, and air-dried prior to use. A geologic sample from Yucca Mountain was collected from an outcropping of the Topopah Spring member of the Paintbrush Tuff. The rock was crushed and sieved between 20 and 60 mesh (0.250−0.841 mm). X-ray diffraction analysis of the tuff identified silicates, feldspar, and an amorphous component, likely glass. Additionally, there were trace concentrations of a phyllosilicate, likely mica or vermiculite. Deionized water (DI) represents the practical lower limit of the solution *I* at the site. The standard formulation of simulated J-13 groundwater (s-J-13) is 0.368 mM Na_2CO_3 and 10.6 mM $NaHCO_3$, pH 7.8 (*19*). Varying dilutions were prepared for colloid settling and

* Corresponding author phone: (509)372-7345; fax: (509)372-7471; e-mail: apg@tricity.wsu.edu.

10.1021/es0015949 CCC: $20.00
Published on Web 07/13/2001

TABLE 1. Chemistry of Transport Solutions

s-J-13	10×	1×	0.1×	0×
I	1.16×10^{-1}	1.16×10^{-2}	1.16×10^{-3}	
av pH	8.8	8.7	8.4	7.6
SD	0.3	0.05	0.0	0.1

coagulation experiments: DI, 0.1×, 0.5×, 0.75×, 1×, 2.5×, 5×, 7.5×, and 10×. The *I* and initial pH of the solutions used in transport experiments at ambient laboratory conditions are summarized in Table 1. The pH indicates an order of magnitude difference in H^+ activity; possible pH effects on colloid transport are addressed with the results.

Carboxyl-modified polystyrene latex (CML) microspheres, 1.055 g cm^{-3}, 0.280 μm i.d., with fluorescent crimson dye (Interfacial Dynamics Corp., Portland OR) were used. This colloid was selected because it is hydrophilic, as are the colloids at Yucca Mountain (*19*), and has a diameter that would move freely through the sand and tuff porous media under appropriate chemical conditions. The concentration of colloids in aqueous solutions was determined using fluorescence spectroscopy (model L550B luminescent spectrophotometer, Perkin-Elmer Corp., Norwalk, CT) with $\lambda =$ 619 and 645 nm for excitation and emission, respectively. The initial concentration, c_o, used in transport experiments was ~4.5 mg/L. Bromide (Br^-, c_o ~5000 mg/L) and pentafluorobenzoic acid (PFBA, c_o ~100 mg/L) were used as conservative tracers to monitor hydrodynamic conditions. Bromide (used initially) concentrations were determined by ion-selective electrode (Orion Research Inc., Beverly, MA). PFBA (adopted due to increased analytical precision) was analyzed directly in the column effluent by online UV detection at 254 nm (model 119, Gilson, Middletown, WI).

Particle Characterization. Average particle size was determined from approximately 20 SEM images of colloid and matrix particles. Electrophoretic mobility of colloid and matrix particles was measured using a Coulter Delsa 440 (Coulter Corporation, Miami, FL). Suspensions were ~1 mg L^{-1}. To provide a measure of matrix surface charge, sand and tuff were ground to <2 μm, which was necessary to minimize the extent that the particles would settle during electrophoretic mobility measurements. It is likely that grinding created new surfaces with greater surface charge density, resulting in an experimental artifact that would overestimate ζ-potential. Triplicate multiangle measurements of mildly sonicated samples were made at four angles (9°, 17°, 26°, and 35°). An NTIS traceable standard was carried through the analysis (the EMPSL7, 3.93 ± 0.36 μm·cm/V·s; standard measured, 3.78 ± 0.05 μm·cm/V·s). The resulting data were numerically analyzed by the Marquadt minimization procedure (*20*). Electrophoretic mobility was converted to ζ-potential using Smoluchowski's equation (*21*); ζ-potential was used as an approximation of the surface potential, Ψ. The *I* of the DI solution was estimated by first measuring the electrical conductivity (EC, S m^{-1}) and then using the empirical relation: $I = 0.013$EC (*22*).

Gravitational Settling and Critical Coagulation Concentration. Colloid settling experiments and determination of the critical coagulation concentration (CCC) were conducted using 4 mg L^{-1} suspensions of colloids prepared in various concentrations of s-J-13. Sonicated suspensions were placed directly in 5-mL cuvettes; fluorescence was measured periodically during a 445-min settling period. On the basis of Stoke's law, the distance that a singlet colloid would settle during this settling period was insignificant, 6.7 e^{-5} m (<0.1% of the 4.5-cm cuvette height). Changes in fluorescence were attributed to reduction in colloid concentration due to aggregates settling out of suspension (colloid−colloid interaction). The settling experiments permitted direct measurement of the CCC, an empirical construct that provides the minimum *I* of a salt solution required to induce coagulation, indicated by a drastic decrease in suspended colloid concentration. DLVO theory accurately predicts trends but not the absolute values of CCC (*23*).

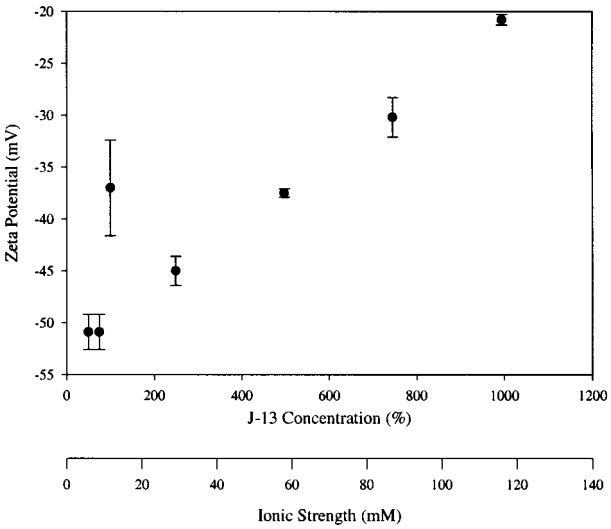

FIGURE 1. ζ-potential of 280-nm latex particles as a function of s-J-13 concentration and *I* (vertical lines represent standard deviation of 12 values).

Transport Method. Miscible displacement experiments were conducted using standard techniques (*24*−*26*). Glass columns, 2.5 cm i.d. (Kontes, Vineland, NJ), were equipped with Teflon bed supports, mesh, and tubing to avoid interaction of the colloids. An infusion pump (AVI Micro 210, AVI, Inc., St. Paul, MN) was used to saturate the columns; to maintain steady-state flow; and to deliver colloid, tracer, and tracer-free solutions. Because of the limited supply of tuff, experiments were executed consecutively on each column. The length, *L*, and bulk density, ρ_b, of the sand (S) and tuff (T) columns were 15.99 cm, 5.60 cm, 1.79 g cm^{-3}, and 1.261 g cm^{-3}, respectively. The volumetric water content, θ (cm^3 cm^{-3}), was determined by mass; the average pore water velocity, *v* (cm h^{-1}), was measured. Tracer and colloid solutions were applied as step inputs to the columns where the pulse size, t_o, is defined as the length of the step input, expressed as the number of column pore volumes. A pore volume, V_w is defined as the volume of water retained within the pore space of the sediment bed. Effluent was collected by automated fraction collector (Br^- and colloids) or analyzed directly (PFBA). The pH of effluent samples was monitored as an indicator of geochemical stability during selected experiments.

Results and Discussion

Particle Characterization. The influence of ionic strength on the ζ-potential of the 280-nm latex particles is presented in Figure 1. The average ζ-potential was −37 mV for 11.6 mM (1× s-J-13); the wider confidence interval indicates variability in the measurement. As expected, increases in *I* caused a near-linear decrease in the absolute ζ-potential values for the latex particles; the deviation from the trend is not explained. The ζ-potentials for the different ionic strength conditions are well within the range of those measured for natural colloids. Colloids from the Savannah River Site, dominated with goethite, kaolinite, quartz, and hydroxy-interlayered vermiculite, had an average ζ-potential of −42 mV (*27*). Dispersible clays collected from surface or near-surface sediment of the New Jersey Coastal Plain had values of about −25 mV (pH 7−10) (*28*); those from the South Carolina Coastal Plain were −41 to −18 mV (*29*).

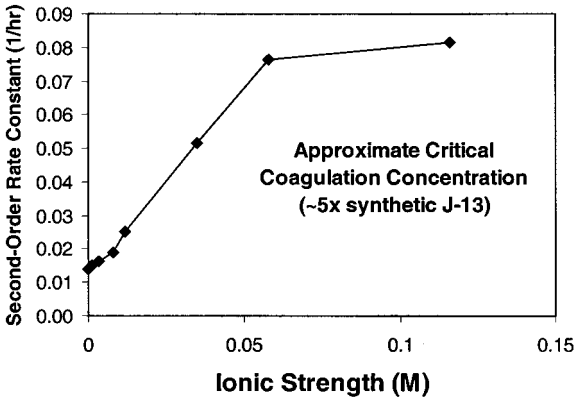

FIGURE 2. Second-order rate constants as a function of ionic strength. Regression analysis was conducted for data ≤58 mol m^{-3}, the approximate critical flocculation concentration.

Gravitational Settling and Critical Coagulation Concentration. Removal of colloids from solution is important because it reduces the potential for off-site colloid-facilitated transport of radionuclides. Second-order rate constants, k, for colloid settling at each I were calculated using

$$\frac{dc}{dt} = -kc^2 \qquad (1)$$

where t is time and k would have units of concn^{-1} time^{-1}. Concentration was expressed in dimensionless form (c/c_o) and the units reduced to h^{-1}. Regression coefficients of the fitted data to the measured values ranged from 0.882 to 0.996, all significant at $P \leq 0.01$. The second-order rate constants are summarized in Figure 2 and increased with increased I up to 0.058 M. A CCC of 0.058 M (5× s-J-13) for the 280-nm latex colloids was measured. In the absence of the transport process and deposition mechanism, colloids are removed from solution by coagulation at ionic strengths equal to or greater than the CCC. The CCC value of 0.058 mol$_c$ L^{-1} is greater than literature values for minerals expected in the Yucca Mountain subsurface, namely, silicates, feldspar, iron oxyhydroxides, zeolites (clinoptilolite and mordenite), and 2:1 minerals (smectite and illites/micas) (*19*, *30*). On the basis of an exhaustive review of literature values, Sumner (*31*) showed that the CCC for smectite and mica was less than ~0.01 mol$_c$ L^{-1} for Na systems and less than ~0.005 mol$_c$ L^{-1} for Ca systems. Removal of natural colloids by coagulation may occur at lower ionic strengths than observed for the model colloids reported here.

Transport Experiments. Results of transport experiments are expressed as breakthrough curves (BTCs), which depict the dimensionless effluent concentration (c/c_o) as a function of cumulative pore volumes eluted. The percent recovery of the analyte was based on the area under the BTC as compared with the measured step input. The fraction of unrecovered colloids was considered to be deposited on the porous media. The retardation factor, R, is defined as the average velocity of water relative to that of the solute or colloid. R values were determined from the area above the BTC (*32*) for all but experiments S-9 and T-5 (the 10× s-J-13 solution on sand and tuff) where low recovery or lack of a clear plateau precluded R calculations. It is important to recognize that colloid deposition in these systems is modeled as an irreversible process and that the retardation factor is based solely on the velocity of the colloids in the effluent (not deposited on the sediment). Measured and calculated parameters are summarized in Tables 2 and 3 for experiments with the conservative tracers and colloids, respectively. The parameters are defined as they are introduced below and are summarized as footnotes in the tables. The experiments are

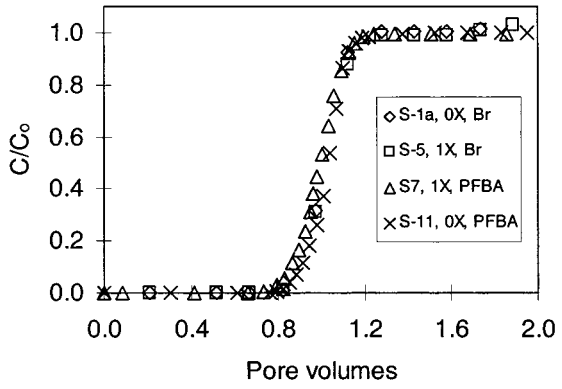

FIGURE 3. Noninteractive tracers in quartz sand showing ideal transport and no change in hydrodynamic conditions for the initial and final experiments (S-1a and S-11).

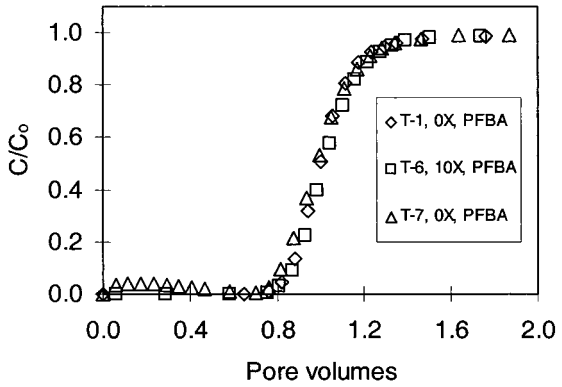

FIGURE 4. Noninteractive tracer in Yucca Mountain tuff showing ideal transport and no change in hydrodynamic conditions for the initial and final experiments (T-1 and T-7).

numbered in the order that they were conducted; the prefix of "S" or "T" represents sand or tuff, respectively; in all cases, full breakthrough curves were generated.

Conservative Tracer Transport. Results of the tracer experiments over the range of ionic strength conditions are shown in Figures 3 and 4, where the pore volume (V_w) axis was truncated at 2.0 to highlight differences. The BTCs appear similar for the different conditions of ionic strength (Table 2); sharp fronts suggest the absence of flow heterogeneities. Recovery was generally 100%; the low recovery of 91% for bromide transport in 1× s-J-13 (S-6) is attributed to analytical error. Retardation factors were approximately 1.0 for 9 out of 10 experiments, as expected for conservative tracers (Table 2). The Peclet number, Pe, characterizes hydrodynamic dispersion, which is normalized for velocity and length, allowing comparison of measurements made under varying conditions. The Peclet number was determined with a nonlinear, least-squares, one-parameter, curve-fitting technique (CFITIM3, University of Florida) based on the Brenner solution to the convection−dispersion equation, CDE (*33*), expressed here in dimensionless terms:

$$R\frac{\partial C}{\partial T} = \frac{1}{Pe}\frac{\partial^2 C}{\partial Z^2} - \frac{\partial C}{\partial Z} - \mu^E C \qquad (2)$$

where C, T, and Z are dimensionless concentration, time, and distance, respectively, and μ^E (also dimensionless) is a first-order decay coefficient. The decay term is zero for conservative tracers (for the colloids, μ^E describes irreversible deposition on the sediment, below). The model fits overlie the experimental BTCs but were omitted from Figures 3 and 4 because they obscured the data. Dimensionless terms are further defined in Table 4, where t is time (h), x is distance

TABLE 2. Experimental Parameters for Conservative Tracer Transport in Sand (S) and Tuff (T) Columns[a]

exp[b]	s-J-13	analyte	θ	V_w (mL)	v (cm h^{-1})	t_o (V_w)	recovery (%)	R	Pe (95% CI)	D (95% CI)
S-1a	0×	Br^-	0.326	25.59	24.4	3.21	99.3	1.01	164 (118−210)	2.38 (1.86−3.30)
S-5	1×	Br^-	0.326	25.59	24.4	3.04	102.0	1.02	234 (175−293)	1.67 (1.33−2.23)
S-6	1×	Br^-	0.326	25.59	24.4	1.83	91.0	1.02	248 (199−296)	1.57 (1.32−1.96)
S-2	0×	PFBA	0.326	25.59	11.6	5.04	100.1	1.08	245 (226−263)	0.76 (0.71−0.82)
S-7	1×	PFBA	0.326	25.59	25.1	3.90	101.1	1.00	183 (131−235)	2.19 (1.71−3.06)
S-8	1×	PFBA	0.326	25.59	37.5	2.50	102.2	0.99	227 (152−302)	2.64 (1.99−3.94)
S-11	0×	PFBA	0.326	25.59	24.4	1.95	106.8	1.02	217 (102−331)	1.80 (1.18−3.83)
T-1	0×	PFBA	0.494	16.43	13.6	4.14	100.0	1.03	59 (39−79)	1.56 (1.16−2.36)
T-6	10×	PFBA	0.496	16.18	13.6	4.18	102.2	1.05	116 (72−159)	0.78 (0.57−1.26)
T-7	0×	PFBA	0.496	16.31	13.6	2.64	96.6	0.99	40 (25−55)	2.28 (1.66−3.65)

[a] θ, average volumetric water content; V_w, average pore volume; v, average pore water velocity; t_o, step input; R, retardation factor, reflecting the velocity of colloids in the effluent ($v_{water}/v_{colloid}$); Pe, Peclet number; D, hydrodynamic dispersion. [b] S, sand; T, tuff; number indicates order that the experiment was conducted.

TABLE 3. Experimental Parameters for Colloid Transport in Sand (S) and Tuff (T) Columns[a]

exp	s-J-13	θ	PV (mL)	v (cm h^{-1})	t_o (V_w)	recovery (%)	R	μ_l (95% CI) (h^{-1})
S-1b	0×	0.326	25.59	24.4	4.87	108.5	1.01	b
S-3	0.1×	0.326	25.59	24.4	3.16	98.2	1.07	0.06 (0.02−0.09)
S-4	1×	0.326	25.59	24.4	3.04	89.3	1.01	0.18 (0.16−0.21)
S-9	10×	0.326	25.59	24.4	3.68	2.9		5.6 (5.4−5.8)
S-10	0×	0.326	25.59	24.4	4.41	107.0	0.95	b
T-2	0×	0.496	13.63	15.81	5.37	102.1	0.87	b
T-3	0.1×	0.492	13.52	15.98	7.99	100.6	0.90	b
T-4	1×	0.493	13.53	15.93	7.99	87.3	0.97	0.43 (0.36−0.49)
T-5	10×	0.496	13.61	15.92	8.45	10.6		7.0 (6.6−7.3)
T-8	0×	0.493	13.53	15.90	8.03	102.6	0.87	b

[a] See Table 4 for parameter definitions; μ_l = first-order rate constant for deposition. [b] Estimate $<6 \times 10^{-9}$ and 95% CI overlapped zero.

TABLE 4. Dimensionless Transport Parameters (ref *35*)

parameters	T	Z	Pe	R	C	μ^E
expressions	vt/L	x/L	vL/D	$v_{water}/v_{colloid}$	c/c_o	$L\mu_l/v$

(cm), D is hydrodynamic dispersion (cm^2/h), v is velocity, μ_l is the first-order decay term (dimensional, h^{-1}), where the subscript l represents the liquid phase; all other terms are as defined previously.

Peclet numbers were somewhat lower for tuff than sand, indicating greater dispersion; the decrease from 59 to 40 between the initial and final experiments on the tuff (T-1 and T-7) was not statistically significant. Increased dispersion on the tuff is likely due to internal porosity, which is noted and reported in another study (*34*). Ionic strength had no effect on retardation, retention, or dispersion of the tracers; hydrodynamic properties did not change appreciably after colloids were displaced and deposited on the sediment. Tracer experiments indicate column performance; the results for the initial and final experiments on the sand also demonstrate that hydrodynamic dispersion did not change following the colloid transport experiments (S-1a as compared with S-11). Recovery >100% for the conservative tracer in experiment S-11 is an artifact due to analytical interference by constituents leaching from the sand, triggered by the change in solution matrix from 10× s-J-13 to DI.

Colloid Transport and Retention. The effect of I on colloid mobility is illustrated in Figures 5 and 6 and quantified in Table 3. The results for experiments S-1b and T-2 in DI water serve as an important control: recovery was ~100%, indicating no deposition on the sediment and that colloids were transported at the velocity of the aqueous solution ($R = 1$). Although the sand column was preequilibrated with >35 pore volumes of DI solution prior to colloid application (S-1b), leachate from the column interfered with colloid analysis in the effluent (c) and was absent from the influent solution (c_o). This resulted in c/c_o >1.0 and >100% recovery (S-1b). This artifact is due to the absence of ions in the influent solution (DI) and was not observed with the s-J-13 solutions. This effect had subsided by the final experiment with the DI solution (S-10), was not observed for the tuff, and was not considered further. The conditions for the final experiment on the sand (S-10) were identical to those of the initial experiment (S-1b); the results (Table 3) indicate that performing multiple experiments on the columns did not change colloid deposition and transport. The most common effect of continued colloid application is "filter ripening" or an increase in colloid removal with time. This would result in a negative slope of the BTC after initial breakthrough and was not observed.

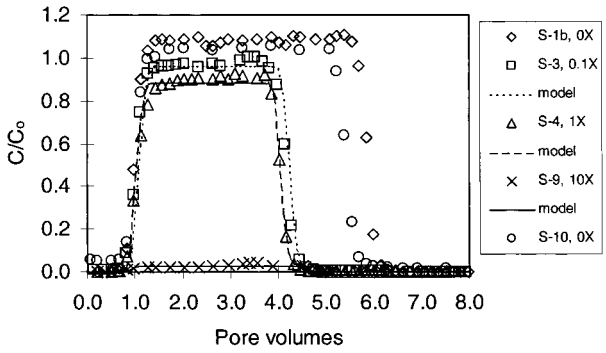

FIGURE 5. Transport and deposition of 280-nm colloids in quartz sand. Plateaus of the BTCs indicate deposition for the 1× and 10× s-J-13 solutions. The lines depict results of curve-fitting with a first-order model for deposition. The data for S-1b, 0× illustrate an experimental artifact (see text for explanation).

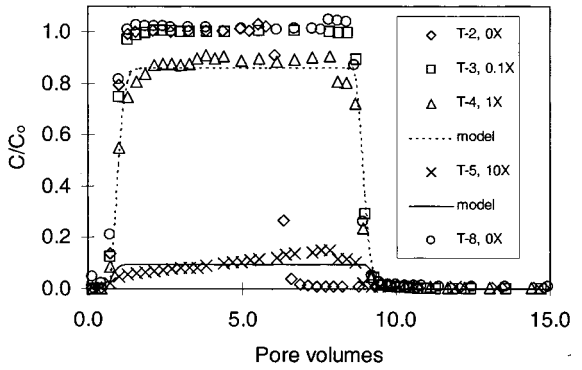

FIGURE 6. Transport and deposition of 280-nm colloids in Yucca Mountain tuff. Plateaus of the BTCs indicate deposition for the 1× and 10× s-J-13 solutions. The increase in slope for the 10× s-J-13 solution (T-5) indicates a decreasing rate of deposition. Lines depict results of curve-fitting with a first-order model for deposition.

Modeling of BTCs was undertaken to determine pseudo-first-order rate coefficients for deposition (*13*, *16*). This approach provides a single parameter that can be readily incorporated into larger-scale transport models that are used for long-term performance assessments such as that for Yucca Mountain. Colloid deposition during transport was modeled using an analytical solution to the CDE, CXTFIT, version 2.1 (*35*). A one-parameter curve-fit was used to determine μ^E (dimensionless) from BTC data, with the exception of the 10× s-J-13 condition, S-9 and T-5, where both R and μ^E were determined by curve-fitting. As mentioned previously, the low mass recovery in the effluent or lack of a clear plateau for the BTC precluded independent estimation of R for several cases. Values of *Pe* were fixed to those determined with conservative tracers, recognizing that due to the size difference, dispersion of the colloid may be less than that of the tracers. Given the limited dispersion in these systems, the difference was ignored.

For DI and 0.1× solutions, colloid deposition was essentially zero (S-1b, S-10, T-2, T-3, T-8). The similarity in colloid transport for DI (pH 7.6) and 0.1× (pH 8.5) solutions indicates that the pH change did not affect colloid transport or deposition. Although deposition is a complex process that is dependent upon a number of factors, agreement between the model and experimental data support its general description as a pseudo-first-order process. For solutions with $I > 0.1\times$, the removal rate coefficient (μ_l) increased from ~0.06 to ~6 h^{-1}, with increasing I from 0.00116 to 0.116 mol L^{-1}, suggesting a linear dependence. Colloid breakthrough for the 10× s-J-13 condition on the tuff (T-5) did not exhibit a flat plateau as observed for the other conditions. The increase in colloid concentration after initial breakthrough (1 V_w) indicates a decreasing rate of deposition. This has been demonstrated for oppositely charged colloid and matrix particles (*36*, *37*) in contrast to the present study where both the colloids and the matrix particles are negatively charged. This is one aspect where deposition on the sand and tuff materials differed and would result in greater colloid transport through the tuff.

A systematic increase in colloid retention on the sediment with increasing I is indicated by the lower percent recovery of colloids in the column effluent and an increase in the rate coefficient for colloid removal (Table 3). The nearly complete removal for the 10× s-J-13 condition is expected based on theoretical estimates of conditions that favor deposition and the CCC (calculations not shown). As noted for the deposition rate coefficients, the mass fraction of colloids retained also appears to increase linearly with increasing I (not surprising as they are both based on mass recovery in the effluent). To further investigate the dependency of colloid removal on I,

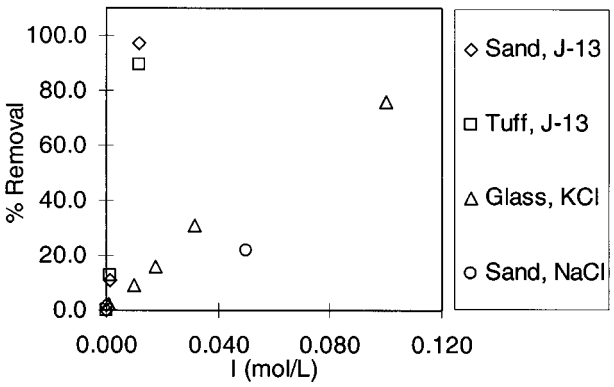

FIGURE 7. Colloid removal during transport and comparison of the results for the model Yucca Mountain system (quartz sand or crushed tuff, s-J-13, 0.280-μm colloids) with those of Elimelech and O'Melia (*14*) (glass, KCl, 0.753-μm colloids) and McDowell-Boyer (*15*) (sand, NaCl, 1.46-μm colloids).

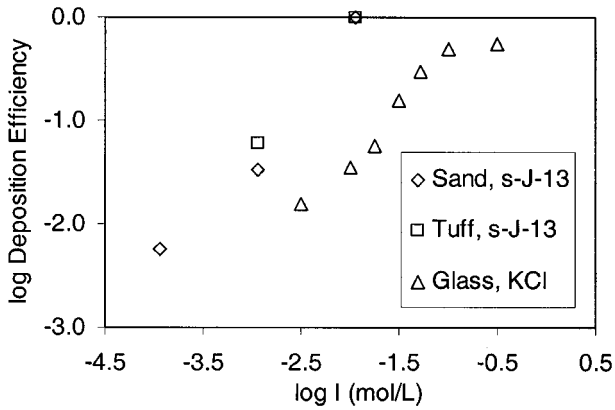

FIGURE 8. Colloid deposition efficiency comparing results for the model Yucca Mountain system (quartz sand or crushed tuff, s-J-13, 0.280-μm colloids) with those of Elimelech and O'Melia (*14*) (glass, KCl, 0.753-μm colloids).

data from the literature were evaluated (Figure 7). These investigations (*14*, *15*) used polystyrene latex microspheres with sulfate functional groups and ζ-potentials ranging from −40 to −90 mV, as compared −20 to −55 mV for the carboxyl-modified spheres used in the present study and −18 to −42 for the natural colloids mentioned previously. Percent removal for literature data was estimated from the plateau or maximum of the BTCs and is plotted in Figure 7 for comparison. At a particular I, removal for our system was greater than that for literature data, likely due to lower repulsive forces associated with the carboxyl-modified spheres used here. The greater range of ionic strengths evaluated by Elimelich and O'Melia (*14*) provides additional support for the linear dependence of colloid removal during transport on I in saturated sediments. To facilitate comparison with the engineering literature, we also expressed our results in terms of the "deposition efficiency" (Figure 8), which is also based on maximum breakthrough and mass recovery in the effluent (*14*, *15*). Consistent with the rate and extent of deposition (above), the deposition efficiency was also greater for the model systems reported here.

The retardation factor, R, is typically used to quantify the process of sorption, which is relatively unimportant compared with deposition. However R is also used to define mobility relative to water flow ($v_{water}/v_{colloid}$); here, R is used specifically to index the velocity of colloids that remained in the effluent and were not deposited on the sediment. Although ionic strength affected deposition, the velocity of the colloids that remained in solution did not vary greatly

from that of the aqueous solution, i.e., R was approximately equal to 1.0; transport of colloids that remained in the effluent was not delayed. Retardation of the colloids was ~0.9 through the tuff at low I. Physical exclusion from smaller pores that remain accessible to water and dissolved solutes could result in R <1; however, this physical effect would be largely independent of I. Anion exclusion is an alternate mechanism that is more consistent with the observation primarily at low I.

On the basis of theoretically (not presented) and experimentally derived values of the CCC (5× s-J-13 or 0.058 M), coagulation may have contributed to colloid removal during transport at 10× s-J-13. Comparison of rate coefficients for reactions of different orders (first-order for deposition, second-order for coagulation) is not straightforward. The half-life for coagulation will increase with time (as c decreases), while that for deposition remains constant. Given the greater magnitude of the rate coefficients for deposition and therefore the shorter half-life, we can conclude that deposition was the dominant process.

In summary, this research shows that colloid transport in a sediment−water system modeled after Yucca Mountain is greatly limited by ionic strength. It is noteworthy that, in these water-saturated systems, colloid deposition was similar on sand and tuff. This demonstrates the dominance of solution chemistry rather than differences in stationary solid surface properties in determining colloid deposition and transport in saturated systems. In the vicinity of the waste form at Yucca Mountain, I will very likely exceed the concentration where colloid suspensions were shown to be stable in the model system. Other competing processes and extreme chemical conditions would have to be considered, but the potential for removal of a large percentage of the colloids from the mobile phase exists. For colloids that migrate to the more dilute far-field, 90% or more of the colloids may move at the velocity of water. The potential for colloid transport as a means of facilitating off-site transport of radionuclides from the Yucca Mountain repository is considered in the performance assessment of the site. Understanding colloid transport in this model system is a step toward making this determination. In light of disagreement between observations and theoretical predictions based on DLVO theory, demonstration of the linear relationship between colloid deposition and I in saturated systems may prove useful.

Acknowledgments

This research was supported by EPRI; the authors greatly appreciate the support of the project director, Dr. John Kessler. Student researchers Kathleen A. David, Jonathan R. Ferris, and Lauren J. Webb assisted with sample analysis. Discussions with Pete McGrail regarding colloid deposition are appreciated. The majority of this research was conducted with the Applied Geology and Geochemistry group at Pacific Northwest National Laboratory, which is operated for the U.S. DOE by Battelle Memorial Institute, under Contract DE-AC06-76RLO 1831. Westinghouse Savannah River Co. is operated for the U.S. DOE under Contract DE-AC09-89SR-18035.

Literature Cited

(1) McCarthy, J. F.; Zachara, J. M. *Environ. Sci. Technol.* **1989**, *23*, 496−502.
(2) Saiers, J. E.; Hornberger, G. M. *Water Resour. Res.* **1996**, *32*, 33−41.
(3) Buddemeier, R. W.; Hunt, J. R. *Appl. Geochem.* **1988**, *3*, 535−548.
(4) Penrose, W. R.; Polzer, W. L.; Essington, E. H.; Nelson, D. M.; Orlandini, K. A. *Environ. Sci. Technol.* **1990**, *24*, 228−234.
(5) Marley, N. A.; Gaffney, J. S.; Orlandini, K. S.; Cunningham, M M. *Environ. Sci. Technol.* **1993**, *27*, 2456−2461.
(6) Kaplan, D. I.; Bertsch, P. M.; Adriano, D. C.; Orlandini, K. A. *Radiochim. Acta* **1994**, *66/67*, 181−187.
(7) Kersting, A. B.; Efurd, D. W.; Finnegan, D. L.; Rokop, D. J.; Smith, D. K.; Thompson, J. L. *Nature* **1999**, *397*, 56−59.
(8) Ramsay, J. D. F. *Radiochim. Acta* **1988**, *44/45*, 165−170.
(9) DOE. *Viability Assessment of a Repository at Yucca Mountain*; DOE/RW-0508; U.S. Department of Energy, Office of Civilian Radioactive Waste Management, Yucca Mountain Site Characterization Office: Las Vegas NV, 1998.
(10) Mann, F. M. *Hanford Immobilized Low-Activity Tank Waste Performance Assessment*; DOE/RL-97-69; UC-2050; 1998.
(11) Meijer, A. A Strategy for the Derivation and Use of Sorption Coefficients in Performance Assessment Calculations for the Yucca Mountain Site. In *Proceedings of the DOE/Yucca Mountain Site Characterization Project Radionuclide Adsorption Workshop at Los Alamos National Laboratory*, September 11−12, l990; Los Alamos National Laboratory Report LA-12325-C; NNA.920819.0077; 1992.
(12) Chang, J. S.; Vigneswaran, S. *Water Res.* **1990**, *24*, 1425−1430.
(13) Tobiason, J. E. *Colloids Surf.* **1989**, *39*, 53−77.
(14) Elimelech, M.; O'Melia, C. R. *Environ. Sci. Technol.* **1990**, *24*, 1528−1536.
(15) McDowell-Boyer, L. *Environ. Sci. Technol.* **1992**, *26*, 586−593.
(16) Saiers, J. E.; Hornberger, G. M. *Water Resour. Res.* **1999**, *35*, 1713−1727.
(17) Elimelech, M. *Water Res.* **1992**, *26*, 1−8.
(18) Song, L.; Elimelech, M. *J. Colloid Interface Sci.* **1994**, *167*, 301−313.
(19) Triay, I.; Simmons, A.; Levy, S.; Nelson, S.; Huttall, H.; Robinson, B.; Steinkampf, W.; Viani, B. *Colloid-Facilitated Radionuclide Transport at Yucca Mountain*; LA-12779-MS; Los Alamos National Laboratory: Los Alamos, NM, 1995.
(20) Cummins, P. G.; Staples, E. J. *J. Langmuir* **1987**, *2*, 1109−1121.
(21) Hiemenz, P. C.; Rajagopalan, R. *Principles of Colloid and Surface Chemistry*, 3rd ed.; Marcel Dekker: New York, 1997.
(22) Griffin, R. A.; Jurinak, J. J. *Soil Sci.* **1973**, *116*, 26−30.
(23) van Olphen, H. *Clay Colloid Chemistry*; Wiley-Interscience: New York, 1977.
(24) Zhong, W. Z.; Lemley, A. T.; Wagenet, R. J. In *Evaluation of Pesticides in Ground Water*; Garner, W. Y., Honeycutt, R. C., Nigg, H. N., Eds.; ACS Symposium Series 315; American Chemical Society: Washington, DC, 1986; pp 61−77.
(25) Gamerdinger, A. P.; Lemley, A. T.; Wagenet, R. J. *J. Environ. Qual.* **1991**, *20*, 67−12.
(26) Gamerdinger, A. P.; van Rees, K. C. J.; Rao, P. S. C.; Jessup, R. E. *Environ. Sci. Technol.* **1994**, *28*, 376−382.
(27) Kaplan, D. I.; Bertsch, P. M.; Adriano, D. C.; Miller, W. P. *Ground Water* **1995**, *33*, 707−717.
(28) Ryan, J. N.; Gschwend, P. M. *Environ. Sci. Technol.* **1994**, *28*, 1717−1726.
(29) Kaplan, D. I.; Bertsch, P. M.; Adriano, D. C.; Miller, W. P. *Environ. Sci. Technol.* **1993**, *27*, 1193−1200.
(30) Meijer, A. *Yucca Mountain Project Far-Field Sorption Studies and Data Needs*; Los Alamos National Laboratory Report LA-11671-MS; UC-510; Los Alamos, 1990.
(31) Sumner, M. E. *Aust. J. Soil Res.* **1993**, *31*, 683−750.
(32) Nkedi-Kizza, P.; Rao, P. S. C.; Hornsby, A. G. *Environ. Sci. Technol.* **1987**, *21*, 1107−1111.
(33) Brenner, H. *Chem. Eng. Sci.* **1962**, *17*, 229−243.
(34) Gamerdinger, A. P.; Kaplan, D. I. *Environ. Sci. Technol.* **2001**, *35*, 2497−2504.
(35) Toride, N.; Leij, F. J.; van Genuchten, M. Th. *The CXTFIT Code for Estimating Transport Parameters from Laboratory or Field Tracer Experiments*, Version 2.1; Research Report 137; U.S. Salinity Laboratory, Agricultural Research Service, U.S. Department of Agriculture: Riverside, CA, 1995.
(36) Liu, D.; Johnson, P. R.; Elimelech, M. *Environ. Sci. Technol.* **1995**, *29*, 2963−2973.
(37) Johnson, P. R.; Sun, N.; Elimelech, M. *Environ. Sci. Technol.* **1996**, *30*, 3284−3293.

Received for review August 15, 2000. Revised manuscript received May 14, 2001. Accepted May 16, 2001.

ES0015949